LA-UR-14-27335
Approved for public release; distribution is unlimited.

Title: Measurement of reaction-in-flight neutrons using thulium activation at the National Ignition Facility

Author(s): Grim, Gary P.
Rundberg, Robert S.
Hayes-Sterbenz, Anna Catherine
Jungman, Gerard
Boswell, Melissa
Klein, Andreas
Wilhelmy, Jerry B.
Tonchev, Anton
Yeamans, Charles
Fowler, Malcolm M.

Intended for: SPIE Optics & Photonics 2014 - Target Diagnostics Physics and Engineering for ICF III Conference, 2014-08-17 (San Diego, California, United States)

Issued: 2014-09-23 (rev.1)

Measurement of reaction-in-flight neutrons using thulium activation at the National Ignition Facility

G. P. Grim,[a] and R. Rundberg,[a] M.M. Fowler,[a] A. C. Hayes,[a] G. Jungman,[a] M. Boswell, [b] A. Klein,[a], J. Wilhelmy[a], A.P. Tonchev,[b] and C. B. Yeamans,[b]

[a]Los Alamos National Laboratory, PO Box 1663, Los Alamos, NM 87545, USA
[b]Lawrence Livermore National Laboratory, 7000 East Rd., Livermore, CA 94551, USA

ABSTRACT

We report on the first observation of tertiary reaction-in-flight (RIF) neutrons produced in compressed deuterium and tritium filled capsules using the National Ignition Facility at Lawrence Livermore National Laboratory, Livermore, CA. RIF neutrons are produced by third-order, out of equilibrium ("in-flight") fusion reactions, initiated by primary fusion products. The rate of RIF reactions is dependent upon the range of the elastically scattered fuel ions and therefore a diagnostic of Coulomb physics within the plasma. At plasma temperatures of ∼5 keV, the presence of neutrons with kinetic energies greater than 15 MeV is a unique signature for RIF neutron production. The reaction ^{169}Tm(n,3n)^{167}Tm has a threshold of 15.0 MeV, and a unique decay scheme making it a suitable diagnostic for observing RIF neutrons. RIF neutron production is quantified by the ratio of ^{167}Tm/^{168}Tm observed in a ^{169}Tm foil, where the reaction ^{169}Tm(n,2n)^{168}Tm samples the primary neutron fluence. Averaged over 4 implosions[1–4] at the NIF, the ^{167}Tm/^{168}Tm ratio is measured to be $1.5 \pm 0.3 \times 10^{-5}$, leading to an average ratio of RIF to primary neutron ratio of $1.0 \pm 0.2 \times 10^{-4}$. These ratios are consistent with the predictions for charged particle stopping in a quantum degenerate plasma.

Keywords: Neutron time-of-flight, Inertial Confinement Fusion, Scintillators

1. INTRODUCTION

In high-energy density implosions at facilities such as the National Ignition Facility[5] (NIF), deuterium and tritium filled capsules are routinely compressed to temperatures of ∼ 5 KeV, and pressures of 100 Gbar[1,2] producing a $O(10^{16})$ fusion reactions. A dominant nuclear reaction in these experiments is T(D,n)α, resulting in a 14.1 MeV neutron and a 3.5 MeV alpha particle. Since the speeds of the products are much greater than the sound speed of the plasma, these particles, and the reactions they initiate, may be used to probe the surrounding plasma that initiated the fusion reactions.

In particular, the stopping of charged particles in a plasma may be inferred by measuring the rate of out-of-equilibrium fusion reactions produced by an implosion. This processes is illustrated in Fig. 1 where a fast neutron, or alpha particle, elastically scatters a thermal ion, imparting kinetic energy. If this knock-on ion undergoes a fusion reaction prior to thermalization, the daughter neutron and alpha particle will be produced

Send correspondence to: E-mail: gpgrim@lanl.gov, Telephone: 1 (925) 423-1058

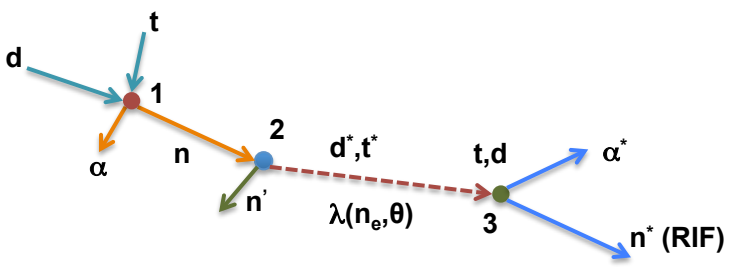

Figure 1: Tertiary reaction chain to produce high energy neutrons in a DT plasma.

in a moving frame of reference. Elastic scatters of 14.1 MeV neutrons with deuterium and tritium results in a ion birth spectrum which reaches kinematic endpoints of 12.5 MeV and 10.6 MeV respectively. A subsequent fusion reaction of a super-thermal and thermal ion pair, will result in a reaction-in-flight (RIF) neutron, with lab kinetic energy ranging from 9.5 MeV to 30 MeV.

The rate of RIF neutron production, which has been calculated elsewhere,[6] is strongly dependent on the range of the knock-on fuel ion. This may be seen through Eqns. 1, and 2. Eqn. 1 is the intensive spectral rate of RIF neutron production and is given by folding the fusion cross section, σ_{DT}, a kinematic factor,dF/dE_{RIF}, which corrects for the lab frame transformation and counting only high-energy neutrons, and the knock-on fuel ion spectrum, $d\psi_{ko}/dE_{ko}$. The knock-on spectrum is not the birth knock-on spectrum, but the charged particle modulated spectrum which is calculated in Eqn. 2. Under the assumption that the volume of knock-on scatters is large when compared to density and temperature variations, as well as charged particle stopping length, *e.g* the dense DT fuel, the knock-on spectrum is proportional to the local flux of 14 MeV neutrons (ψ_{14}), the fuel density (n_{DT}) and knock-on cross section, and inversely proportional the plasma stopping of the fuel ions (E_f). Further, each energy, E_f, in the modulated spectrum sums over all larger birth energies E_o, where the ions have undergone a sufficient number of collisions to have induced a change in their kinetic energy of $\partial E_o/\partial E_f$.

$$\frac{d\Gamma_{RIF}}{dE_{RIF}dV} = n_{DT}\int_0^{E_{ko}^{max}} dE_{ko}\frac{d\psi_{ko}}{dE_{ko}}\sigma_{DT}\frac{dF}{dE_{RIF}} \tag{1}$$

$$\frac{d\psi_{ko}}{dE_{ko}}(E_f) = \frac{\psi_{14}n_{dt}\sigma_{ko}}{|dE/dx(E_f)|}\int_{E_f}^{E_{0max}} dE_0 q_0(E_0) \tag{2}$$

The impact of stopping on the knock-on spectra are shown in Fig. 2. Fig. 2a shows the DT knock-on spectra, at birth, for both deuterons (black) and tritons (red). As each knock-on ion will have a finite range within the plasma, the true knock-on spectrum observed by fuel ions will include contributions from all birth energies greater and have slowed to the observed energy. Fig. 2b shows the true knock-on spectra after the birth spectrum is modulated by stopping in the plasma. The stopping formalism used for this calculation is that of Maynard-Deutsch,[7] which includes a quantum mechanically correct description of charged particle stopping in a degenerate plasma. As can be seen in Eqn. 1, the rate of RIF production, relative to primary neutron fusion, is a function the of knock-on spectrum and therefore a function of stopping in a plasma.

In the following we report on the first observation of RIF neutrons in a ICF/HED experiments. In section 2 we describe the measurement technique, starting with an overview of different approachs, and then focusing on thulium activation. In Sec. 3 we discuss the requirements for observing and measuring thulium activation foils, and the detector system needed to measure the signals of interest, as well as a description of the LANL, 4π clover system that meets these requirements. Following this we present data showing the first observations of RIF neutrons in section 4 and then summarize in section 5.

2. MEASURING RIF NEUTRONS

Typical NIF implosions produce plasma conditions with ion temperatures less than 5-6 keV, generating an approximately gaussian primary neutron energy spectrum with mean energy of roughly 14.1 MeV, and standard deviation ∼180 keV. The fraction of primary neutrons above 15 MeV in the spectrum is less than $\sim 3 \times 10^{-7}$, thus the observation of a production rate above this level must be due to fusion reactions-in-flight. Methods and experiments for observing RIF neutrons have been discussed in past literature[8,9] including both radiochemical activation[6,10] and nToF techniques.[11,12] Because of the tertiary reaction sequence, and the need for substantial areal density, previous searches for RIF neutrons have been unsuccessful. Analytic calculations, as well as computer simulations, indicate the expected fraction of RIF neutrons with $E_n \geq 15$ MeV, relative to the primary, 14.1 MeV neutrons, should be in the range of 1–3 $\times 10^{-4}$.[8,13]

There are several challenges for observing these high energy neutrons using traditional neutron time-of-flight techniques (nToF). In particular, to accommodate the relative production rate requires a detector with a dynamic

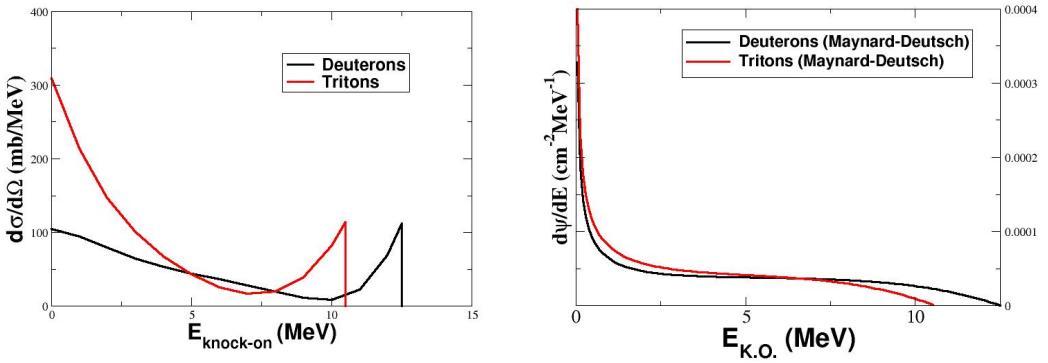

(a) Birth knock-on spectra (b) Stopping modulated knock-on spectra

Figure 2: Knock-on spectra of deuterons and tritons. Fig. 2a shows the birth knock-on spectra for deuterons (black) and tritons (red) after interacting with a 14.1 MeV neutron. Fig. 2b shows the knock-on spectra after modulation due to stopping in the plasma. Each energy in the modulated spectra integrates contributions from all birth energies greater, depleting the high energy portion of the spectrum.

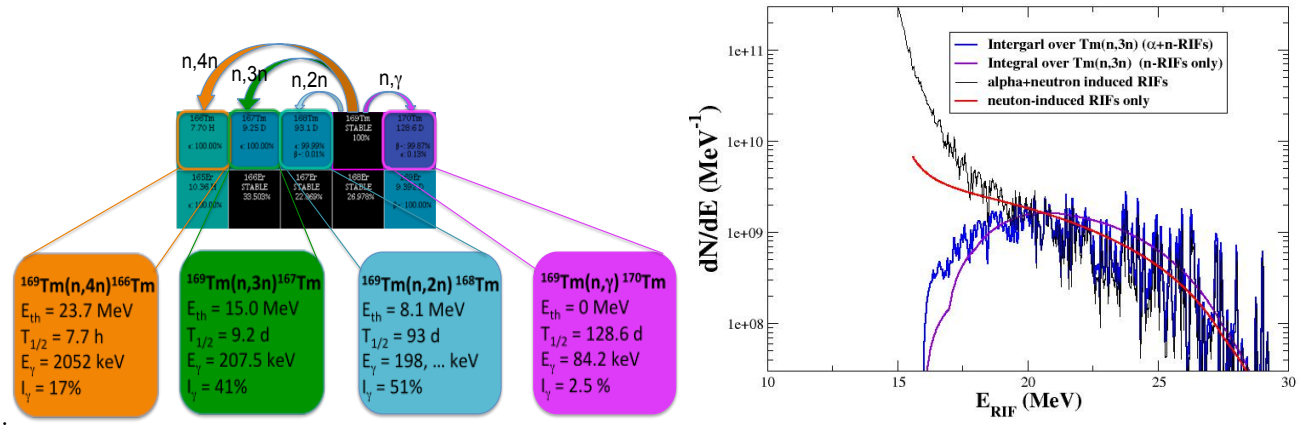

.

(a) Thulium Isotopes (b) Thulium sampled RIF spectrum

Figure 3: Fig. 3a shows the isotopes of thulium. The signature for RIF neutrons is the production of the ^{167}Tm isotope. Fig. 3b shows the expected spectra from a NIF ignition capsule. The black and red curves are a rad-hydro simulation and analytic estimates, using expected densities, temperatures, and reactivities. The blue and purple are the black and red curves folded with the ^{167}Tm differential cross section. The mean neutron energy sampled by ^{167}Tm production is approximately 21 MeV.

range that is greater than 10^4. Although this may be accomplished by viewing a single organic scintillator, of suitable solid-angle and columnar density, using multiple gated photo-detectors, non-trivial systematic corrections due to the different detector impulse response functions and gate timings will naturally result. Further, and most significantly, backgrounds integrated by the scintillator from (n,n'γ) reactions within the nToF flight path can compete with the primary neutron signature, requiring detailed and careful modeling to properly quantify the RIF neutron signal.

As an alternative to nToF techniques, radiochemical activation techniques provide excellent dynamic range and insensitivity to contemporaneous backgrounds at the expense of fine spectral sensitivity. The basic technique is employed by using threshold neutron reactions that integrate over a broad portion of the neutron spectrum. There are a number of possible activation targets that provide a measure of the high-energy neutron spectrum at the NIF, including the ^{12}C(n,2n)^{11}C, ^{197}Au(n,3n)^{195}Au,[6] and ^{169}Tm(n,3n)^{167}Tm, the subject of this work. At present, the respective half-lives of the carbon (20.3 min.) and gold radionuclides (30.5 s & 186.1 d) are not

well matched too the experimental conditions of the NIF, where the timescale for removing activation samples is hours, and results are anticipated within days.

2.1 Thulium Activation

Presently at the NIF, thulium is an excellent compromise to the challenges presented by the carbon and gold RIF neutron diagnostics. Like the gold system, an attractive feature of thulium is its mono-isotopic natural abundance. Fig. 3a shows the thulium isotopes of interest and their dominant production mechanisms, *i.e.* their largest production cross sections, in a NIF experiment. The presence of thulium radionuclides signifies the illustrated nuclear reactions within the foil. In particular, the ^{169}Tm(n,2n)^{168}Tm, and ^{169}Tm(n,3n)^{167}Tm reactions have thresholds of 8.1 and 15.0 MeV respectively. Thus, the abundance ^{168}Tm is a measure of the 14.1 MeV neutron fluence passing through the foil, and the abundance of ^{167}Tm is a measure of the RIF neutron fluence passing through the foil. The ratio ^{167}Tm:^{168}Tm, corrected for the reaction cross sections, provides a measure of the RIF neutron to primary 14.1 MeV neutron production ratio in the experiment.

Fig. 3b illustrates an important feature of the ^{167}Tm sampling of the RIF neutron spectrum. The black and red curves show the neutron spectra expected from a putative NIF ignition type implosion. The black curve shows the spectrum from a rad-hydro simulation of a NIF implosion, which includes contributions from both α and neutron knock-on induced reactions in the capsule, while the red curve is an analytic approximation of the neutron only RIF contribution, using the burn averaged fuel areal-density, material temperatures, and nuclear reactivities. The red and black curves diverge below 18.0 MeV due to the lack of α knock-on reactions in the in the analytic calculation.

The blue and the purple curves are the black and red spectra, convolved with the ^{167}Tm differential cross section. Two important conclusions are drawn from these folded spectra. First, the average neutron energy probed by the ^{167}Tm reaction is approximately 21 MeV, and second, the ^{167}Tm sampling of the high-energy spectrum is, to first order, dominated by the neutron induced reactions. The sensitivity to the α induced knock-on reactions occurs in the region of the spectrum where the ^{167}Tm production is coming out of threshold and is close to a factor of 10 off the peak production of 21 MeV. Thus, the ^{167}Tm reaction is primarily probing the production of RIF neutrons in the colder dense fuel of a NIF ignition capsule.

2.2 Experimental Setup

Fig. 4 shows the experimental setup used to sample the high energy ($\geq$ 15 MeV) neutron spectrum at the NIF. Thulium foils are included in two foil packs, which are placed on the "Solid Radchem Collector" (SRC) assemblies that mount to the NIF diagnostic insertion manipulator. Two different thicknesses of thulium foil have been fielded to date, 0.5 and 2 mm. The foils are typically located in a stack-up with several other activation foils, including Zr, In, Al, Ta, and Au. The other foils provide low energy threshold (n,2n) reactions to characterize the spectrum below 14 MeV. The foil pack is housed in a stainless steel assembly and positioned approximately 50 cm from the imploding target. After a high yield NIF shot, the foil assembly is retrieved within a few hours and prepared for assay.

2.3 Signatures of ^{167}Tm and ^{168}Tm Production

Quantification of ^{167}Tm and ^{168}Tm production in a thulium foil exposed to the neutron fluence produced in a NIF experiment is performed using traditional nuclear spectroscopic techniques. As illustrated in Fig. 3a, the half-lives of the ^{168}Tm and ^{167}Tm radionuclides are 93 and 9.25 days respectively. These longer half-lives, allow the samples to be transported from the NIF experimental facility, to a low background counting facility equipped with appropriate radionuclide assay equipment, described further in section 3.

The decay radiation for the two channels of interest are shown in Fig. 5. Both systems decay, virtually 100% of the time, through internal conversion to an excited state of either ^{167}Er, or ^{168}Er. Fig. 5a shows the full network of radiative transitions produced by the ^{168}Er system initiated by ^{168}Tm decays. Unlike the ^{167}Er system, this isotope is quite complicated, with numerous levels above the 207.8 keV line of the ^{167}Er system. Care must be taken to ensure that background from ^{168}Er transitions do not contaminate the measurement of the ^{167}Er signature. Fig. 5b shows a zoomed in region of the ^{168}Er transition scheme. Highlighted in the middle of this scheme, is a 4^- to 3^+, 198.3 KeV transition from the 1.09 MeV level above ground, which has a relative

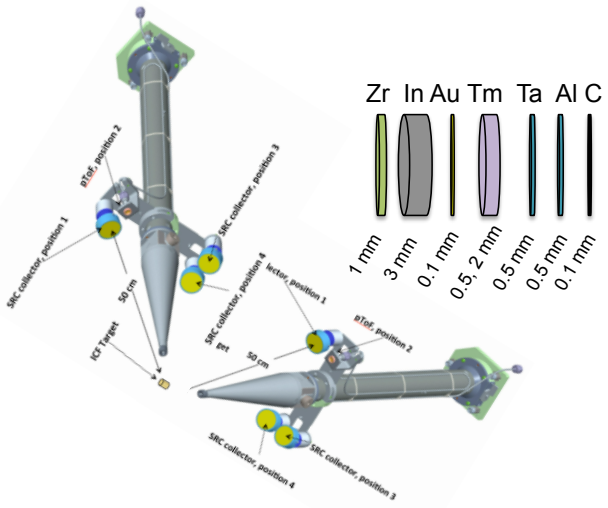

Figure 4: Experimental setup of thulium activation at the NIF. Thulium foils are placed in "SRC" foil pack assemblies and mounted on diagnostic insertion manipulators to be positioned 50 cm from the neutron source. Two assemblies are available for fielding and my be oriented approximately 90 degrees from each.

intensity of 46.6%. This transition is meta-stable with a 1 μs half-life. The photo-peak energy and meta-stable properties of this transition are similar to the ^{167}Er transition, discussed below, and is used to quantify the ^{168}Tm abundance.

As can be seen in Fig. 5c, there are several radiative transitions of the excited ^{167}Er system, with 69% of these passing through the 2s half-life, $1/2^-$ state, resulting in a 207.8 keV photon. This relatively strong radiative decay provides a good signature for assay of ^{167}Tm.

3. LANL 4π CLOVER SYSTEM

Simultaneous assay of ^{168}Tm and ^{167}Tm radionuclides produced in a typical ICF implosion at the NIF places challenging requirements on the detector system used to observe the ^{167}Tm induced gamma transitions. In particular, the neutron spectrum passing through the ^{169}Tm foil, folded with the (n,2n) and (n,3n) reaction cross sections, will result in roughly 10^5 more ^{168}Tm than ^{167}Tm nuclides. Even with the factor of 10 leverage provided by the half-life differences, the subsequent ^{168}Tm actvitiy will generate a substantial Compton continuum, which must be suppressed. Further, a primary ^{168}Tm photo-peak, at 198.3 KeV resides just 9.5 keV below the primary ^{167}Tm signature, and there are a number of $\sim$6 keV X-rays that may sum with the ^{168}Tm photo-peak and potentially contaminate the ^{167}Tm peak.

To suppress contamination and address the flux of Compton scattered electrons, the detector system used must have all of the following characteristics:

- Large acceptance,
- High efficiency,
- Excellent energy resolution,
- Excellent timing resolution,
- Rejection of escaped energy,

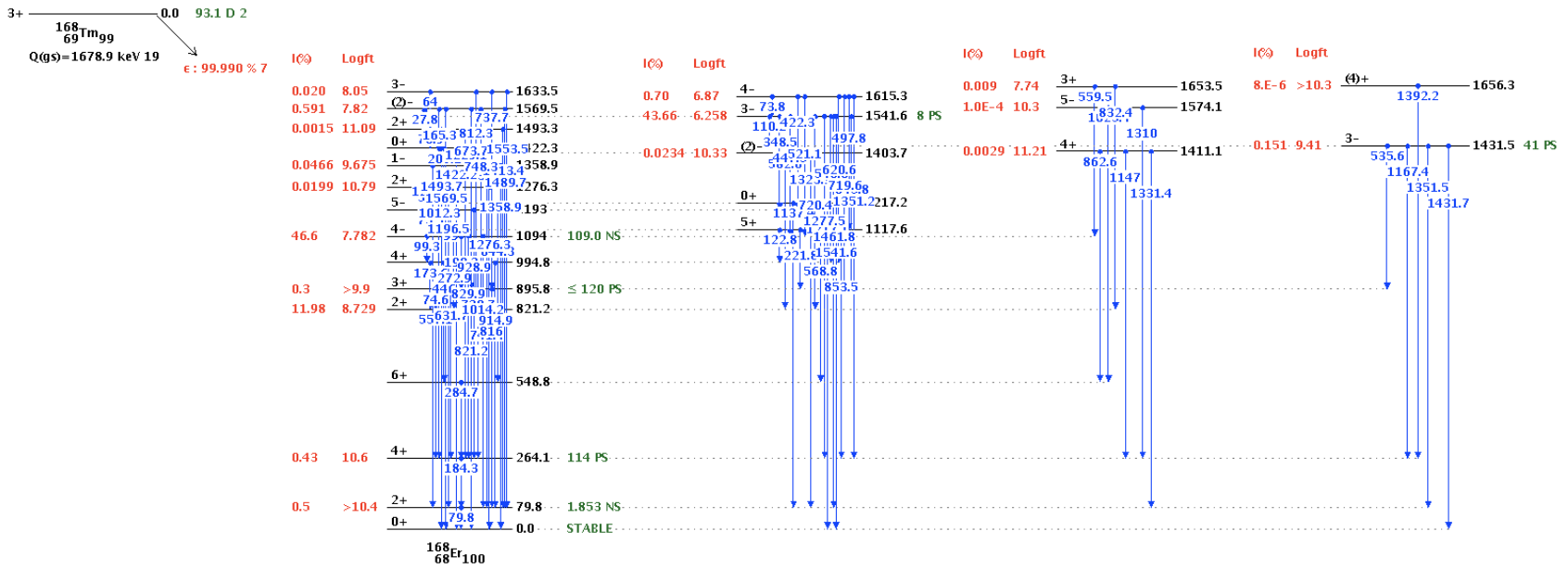

(a) Full ^{168}Tm decay scheme

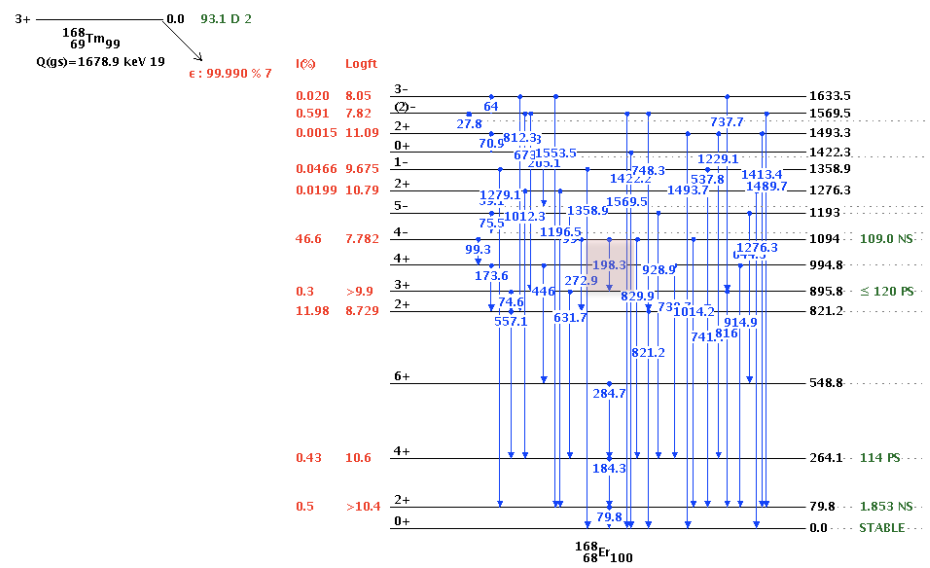

(b) ^{168}Tm decay scheme (zoom).

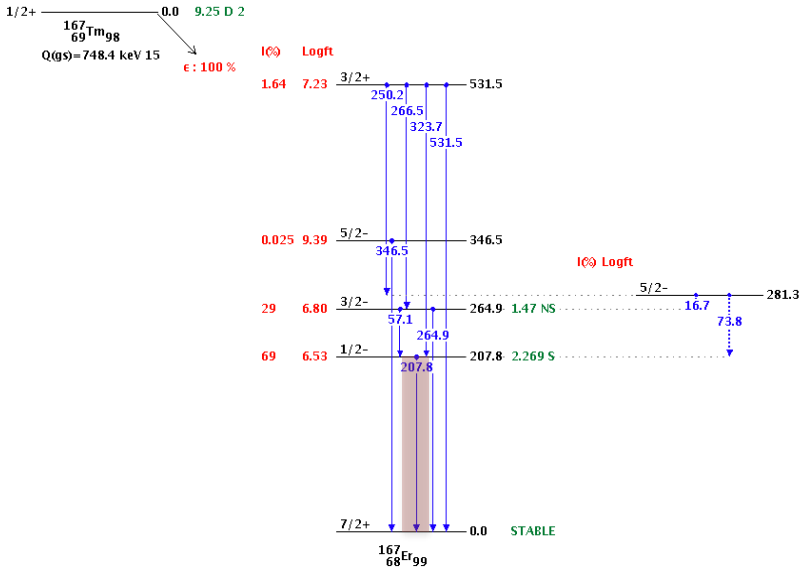

(c) The ^{167}Tmdecay scheme

Figure 5: Radiative decays of the ^{167}Tm and ^{168}Tm systems. The upper figureshows all ^{168}Er transitions, while the figure on the lower left zooms into the transitions of interest for assay of ^{168}Tm decays. The lower right figure shows the primary detection channel for assay of ^{167}Tm. The 69% intense, 208.7 keV transition to the ^{167}Er ground state is the photo-peak of interest for RIF detection.

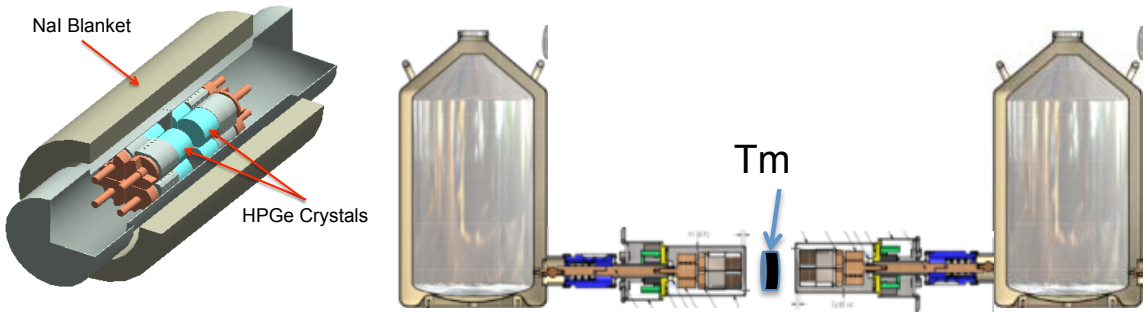

(a) High purity Ge clover model. (b) LANL 4π HPGe detector.

Figure 6: Models of the LANL 4π clover detector. The system is constructed out of eight, 55 mm dia. $\times$ 70 mm long HPGe detector crystals and surrounded by a 2" thick annular blanket made from Tl doped NaI scintillator. The two HPGe clover detectors are configured opposite each other to provide 4π coverage.

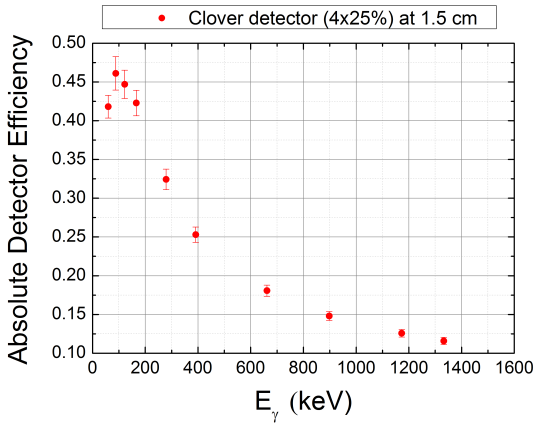

Figure 7: Photo-peak efficiency of the LANL 4π spectrometer.

Fig. 6a shows a model of the LANL 4π clover detector system, designed to meet these criteria. To provide maximum coverage and high efficiency, a set of four, 55 mm diameter by 70 mm long HPGe crystals are arranged in a "clover" geometry to create a ~100 mm dia. $\times$ 70 mm thick detector volume, illustrated in Fig. 6a. The two clover detectors are configured in an opposing view geometry to provide an almost 4π detector volume when viewing thin, 50 mm, samples as illustrated in Fig. 6b. Signals from each of the 8 individual HPGe crystals are digitized and timestamped independently and written to a list mode file. This parallel list mode data stream is post-processed to reconstruct events that occur within the entire 4π detector. This segmentation of the detector and time stamped data stream allows for offline optimization of signal efficiency, as well as summing of multiple, coincident interactions within the detector, thereby suppressing the Compton continuum and optimizing the reconstruction of photo-peaks that initiate cascade decays.

Another strategy to suppress the Compton continuum is addressed by the NaI veto detector, also shown in Fig. 6a. The two opposing HPGe clover detectors are surrounded by a 2 in. thick, Tl doped NaI annular detector. This detector acts as a veto for any energy escaping the HPGe volume, or entering from outside. The NaI annulus is also segmented into 8 separate readout channels with the data processed in a similar manner as the individual HPGe detectors. To reduce environmental backgrounds, the entire system has been located in a shielded room, comprised of several feet of pre-World War II battleship steel. Further, where possible materials, such as the NaI, were specified to be made from very low background feed stock. The space frame supporting the detector was constructed from PEEK to provide a rigid, low mass support and therefore low background as well. The background count rate within the facility is less than 0.2 counts/min.

To maintain excellent resolution, the HPGe crystals are cooled with liquid nitrogen. Energy resolution of the system is typically 1.3 to 1.8 keV over the spectral range from 50 – 3000 keV. The photo-peak efficiency over the

same range is shown in Fig. 7. For the current analysis, the system is ∼40% efficient for the 198.5 and 207.8 keV photo-peaks that signify ^{168}Tm and ^{167}Tm decays respectively.

3.1 Electronics and Data Acquisition

To ensure data quality, appropriate electronics must be used. Bias for the HPGe crystals is supplied by Ortec 660 dual 5K high-voltage power supplies which were designed specifically for HPGe applications. Power for each NaI photo-tube is supplied by a Caen Technologies NDT 1470 HVPS. Signals from each HPGe crystal are directly digitized using an XIA DFG PIXIE-4 digitizer, housed in a National Instruments NI PXI-PCI8336 crate. The digitizers used an input filter time of 12 μs and sampling frequency of 75 MS/s to a depth of 14 bits. NaI photo-tube anode signals are passed through Ortec 113 pre-amps, to bandwidth limit the signal before being sent through the same digitization path. Digitization is initiated by leading-edge discrimination within the digitizer, which results in a potential time walk of ∼50 ns. The channel-to-channel timing resolution of the 16 digitizers used is 13.5 ns. The digitized data are temporarily buffered on board before being transferred through the PIXIE backplane to list mode files using custom DAQ software, written in C, running on an external Linux based computer. One file per detector channel is written for a total of 16 files.

4. EXPERIMENTAL RESULTS

4.1 Sample Spectra

After each assay run, a gamma spectrum is generated by appropriately time correlating and summing energy from each crystal, as appropriate, as well as rejecting any event with non-zero energy in the Compton suppressor. Fig. 8 shows an example spectrum collected by the system viewing a Tm foil exposed neutrons from a NIF ignition experiment. The spectral region shown is from 100 keV to 600 keV. Numerous photo-peaks are present within this spectrum, most of which are either direct photo-peaks from ^{168}Er transistions, sum peaks of cascades of these transitions, or electron-capture coincidences which initiated the decay. For perspective, the inset graphic shows the significant 207.8 keV photo-peak and the region of the spectrum from which it came. Fig. 9 plots the ^{168}Tm and the ^{167}Tm photo-peaks from Fig. 9b on a linear scale and shows the Gaussian fits to the data. The fit to the ^{168}Tm photo-peak results in a mean of 198.5 keV, while the fit to the mean of the ^{167}Tm photo-peak is 207.9 keV, which are both slightly higher than the published values of 198.3 keV and 207.8 keV, for these peaks, but are in good agreement with these values. The ratio of the photo-peak areas is approximately 1×10^{-3}, illustrating the power of an activation technique for measuring signals over a large dynamic range.

As a consistency check, Fig. 10 shows the measured ^{167}Tm activity as a function of time. The horizontal axis is time, given in days since the shot, or zero time. The two graphs show the data from the 2.0 mm, Fig. 10a, and 0.5 mm, Fig. 10b, foils. Within each plot, the color indicates data from a specific shot. Linear fits, using lines with a 9.25 day slopes show good agreement with the data. The intercept indicates activity at zero-time, and correlates well with measured yields of the experiment. Fig. 10b illustrates the improved signal-to-noise performance of the thinner foils. The self attenuation of the thicker foils creates creates larger uncertainty the activity determination.

4.2 Backgrounds

There are two known potential background sources of ^{167}Tm signal that are not from RIF neutron reactions. These potential backgrounds include direct production of ^{167}Tm through the reaction, ^{169}Tm(γ,2n)^{167}Tm, and potential faux ^{167}Tm signals, like ^{237}U decays, produced by ^{238}U (n,2n)^{237}U reactions from within the foil. The ^{237}U nuclide produces an almost indistinguishable 207.8 keV photon, though with a 6.75 day half life.

In deuterium-tritium implosions at the NIF, the flux of high-energy ($E_\gamma \geq 15$ MeV) gammas is dominated by T(d,n)α fusion reactions which pass through the ^{5}He* excited state, and which has been measured in ICF implosions to be $4 \pm 2. \times 10^{-5}$.[14] Further, the ^{169}Tm(γ,2n) cross section at 16.7 MeV is estimated to be 150 mb. Thus, the anticipated contribution to the ^{167}Tm to ^{168}Tm ratio from this background is expected to be less than 3×10^{-6}.

Vendor provided assay of the ^{169}Tm foil shows no measurable ^{238}U present in the foils used in the experiments. As an upper limit on possible ^{237}U contamination, the natural abundance of ^{238}U in the average continental

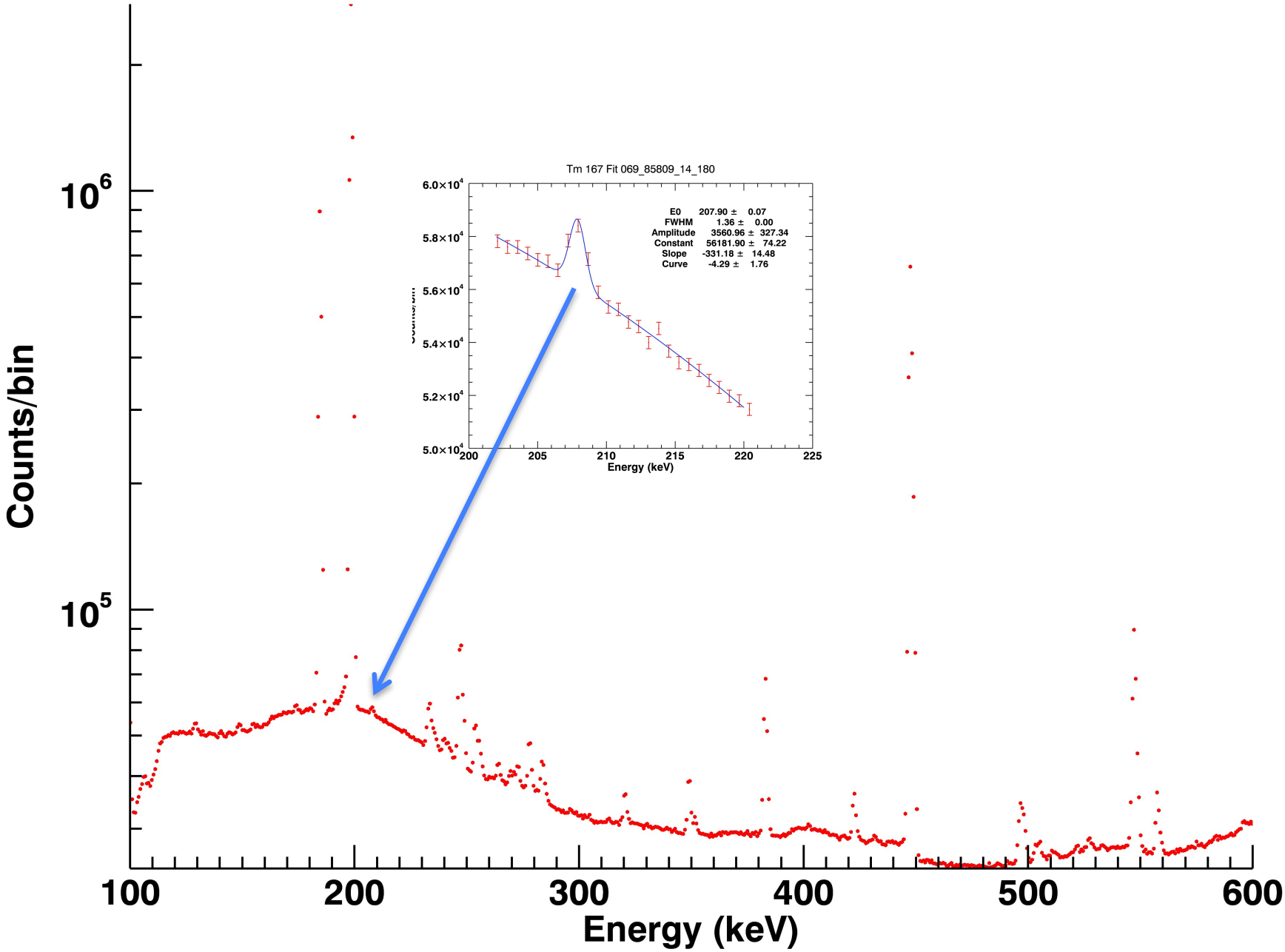

Figure 8: Gamma spectra collected from a ^{169}Tm foil exposed to a NIF ignition experiment and assayed by the LANL 4π clover detector. The inset shows a zoomed in region of the spectrum showing the 207.8 keV ^{167}Tm decay photo-peak.

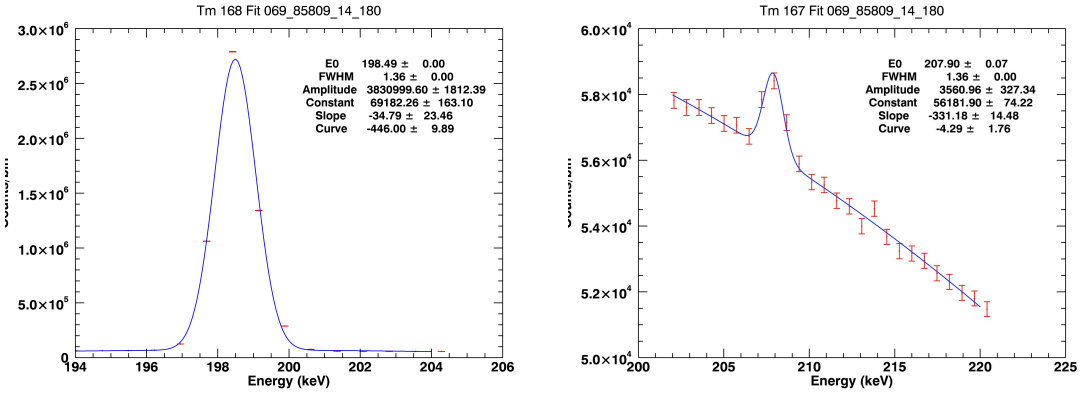

(a) The 198.5 keV photo-peak from the decay of ^{168}Tm.

(b) The 207.8 keV photo-peak from the decay of ^{167}Tm.

Figure 9: Decay spectra collected by the LANL 4π clover detector, zoomed in too the ^{167}Tm and ^{168}Tm decay regions.

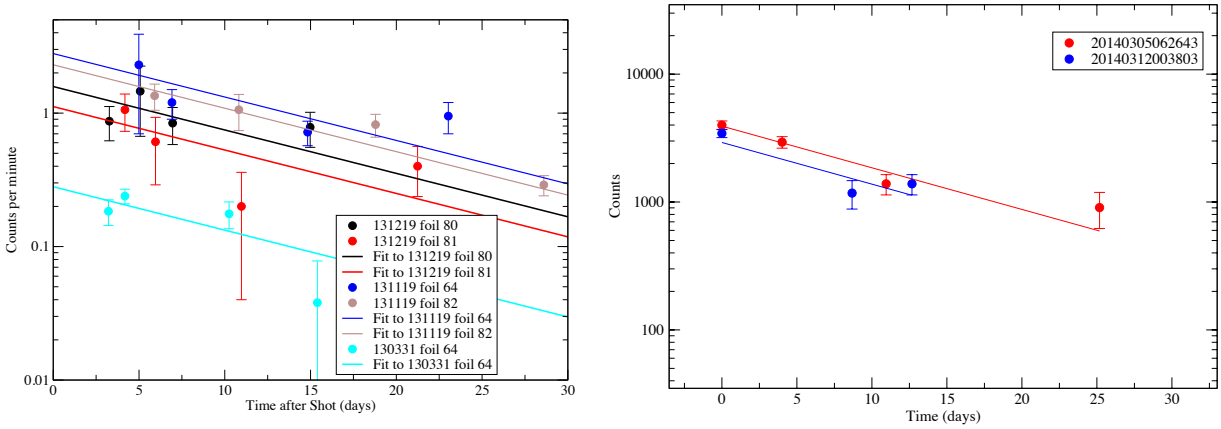

(a) Activity 2.0 mm foils.

(b) Activity 0.5 mm foils.

Figure 10: Activity as a function of time since the shot. Fig. 10a shows the data using 2.0 mm Tm activation foils. Fig. 10b shows the data for the 0.5 mm Tm activation foils.

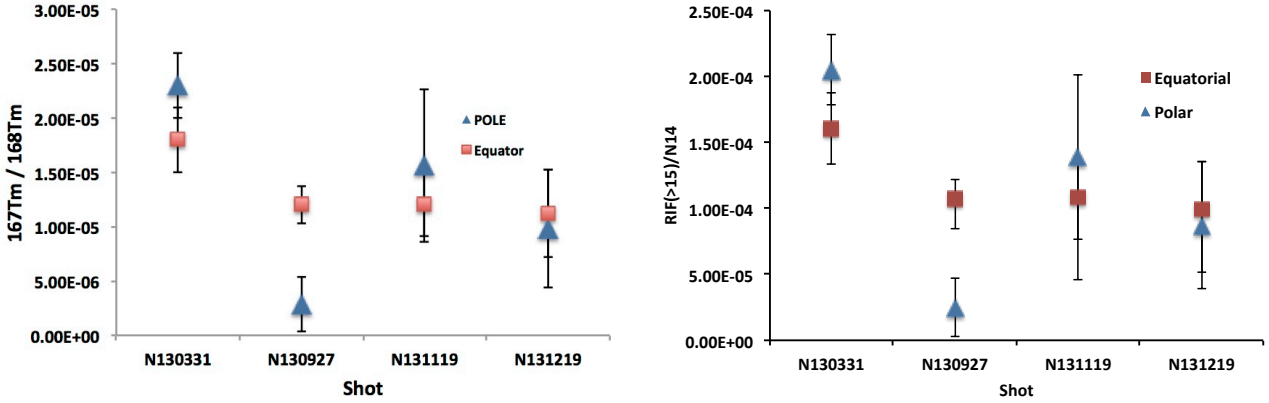

(a) ^{167}Tm to ^{168}TmRatio (b) RIF ($E_n \geq 15$ MeV) to Primary ($E_n \geq 8$ MeV)

Figure 11: The ratios ^{167}Tm to ^{168}Tm and RIF to primary neutrons from four NIF ignition experiments. Fig. 11a shows the ratio of ^{167}Tm to ^{168}Tm, while Fig. 11b corrects for the (n,2n) and (n,3n) differential cross sections to provide a measure of the fraction of RIF neutrons produced in the experiments.

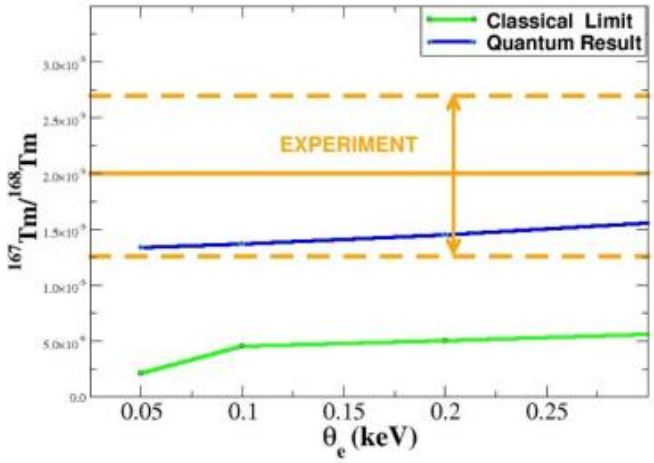

Figure 12: Comparison of the measured ^{167}Tm to ^{168}Tm ratio with analytic calculations of the ratio using both classical and quantum charged particle stopping models. The data are consistent with quantum stopping in the dense deuterium-tritium plasma.

crust of 1.25 ppm[15] may be assumed. Using this atom fraction and the ENDSF-VII ^{238}U(n,2n) cross section data, the relative production of ^{237}U to ^{168}Tm is expected to be less than 6×10^{-7}.

4.3 First Results

Fig. 11a shows the results of ^{167}Tm to ^{168}Tm production in four NIF ignition experiments. Two foils were fielded on each shot, one on the equator (red squares) and one on the pole (blue triangles), *c.f.* Fig. 4. The average ratio of these data are $1.5 \pm 0.3 \times 10^{-5}$. Fig. 11b shows the data in Fig. 11a corrected for the differential cross section to provide a measure of the fraction of RIF neutrons ($E_n \geq 15$ MeV), to primary neutron fluence. The average over the four shots shown is $1 \pm 0.2 \times 10^{-4}$. These measurements are the first reported observation of RIF neutrons in an ICF experiment. The positive observation of RIF neutrons is a significant step forward in the diagnosing of high energy density plasma conditions in implosions at the NIF.

Fig. 12 illustrates the diagnostic power of RIF neutrons. The gold line in Fig. 12 shows the average measured ^{167}Tm to ^{168}Tm ratio from shot N130331, plotted in gold and with the 1-σ envelope included. Using

the other nuclear diagnostic data measured on this shot, including the total neutron yield, ion temperature, down scattered neutron spectrum, and hot-spot size, an estimate of the expected ^{167}Tm to ^{168}Tm ratio is calculated as a function of the electron temperature in the dense deuterium-tritium shell surrounding the hot-spot for two different stopping models. The green curve is the expected ratio for a classical stopping model, and the blue curve shows the expected ratio for a stopping model that includes quantum effects, which are important for a degenerate system. As can be seen from the Fig. 12, the data are consistent with a quantum stopping model in the degenerate deuterium-tritium plasma. In a quantum degenerate plasma, electrons at levels below the Fermi energy do not participate in Coulomb collision that slow kock-on fuel ions, increasing their range, and therefore increasing the probability they will undergo a subsequent tertiary, reaction-in-flight fusion reaction.

5. SUMMARY

Tertiary reaction-in-flight neutrons are a valuable diagnostic for diagnosing the plasma conditions of high energy density implosions at the National Ignition Facility. RIF neutrons, which are suppressed relative to primary neutrons, may be accurately diagnosed using threshold neutron reactions in a suitable activation foil. We report on the first observation of RIF neutrons using the reaction ^{167}Tm(n,3n)^{168}Tm, which has a threshold of 14.8 MeV. Assay of 0.5 and 2.0 mm Tm foils were performed using LANL's 4π clover detector. Taking an average over four NIF ignition implosions, the ratio of ^{167}Tm to ^{168}Tm activity produced at shot time was measured to be $1.5 \pm 0.3 \times 10^{-5}$, resulting in a RIF to primary neutron ratio of $1 \pm 0.2 \times 10^{-4}$. These results were used to confirm that a stopping model that includes quantum effects is required for modeling charged particle transport in the dense deuterium-tritium volume of a NIF ignition implosion.

REFERENCES

1. S. H. Glenzer, D. A. Callahan, A. J. Mackinnon, J. L. Kline, G. Grim, E. T. Alger, R. L. Berger, L. A. Bernstein, and et al., "Cryogenic thermonuclear fuel implosions on the national ignition facility," *Physics of Plasmas* **19**(056318), pp. 056318–1 (15 pp.), 2012.
2. A. J. Mackinnon, J. L. Kline, S. N. Dixit, S. H. Glenzer, M. J. Edwards, D. A. Callahan, N. B. Meezan, S. W. Haan, J. D. Kilkenny, and T. Doeppner, "Assembly of high-areal-density deuterium-tritium fuel from indirectly driven cryogenci implosions," *Physical Review Letters* **108**(215005), pp. 215005–1 (4 pp.), 2012.
3. O. A. Hurricane, D. A. Callahan, D. T. Casey, P. M. Celliers, C. Cerjan, E. L. Dewald, T. R. Dittrich, T. Doppner, D. E. Hinkel, L. F. B. Hopkins, J. L. Kline, S. Le Pape, T. Ma, A. G. MacPhee, J. L. Milovich, A. Pak, H. S. Park, P. K. Patel, B. A. Remington, J. D. Salmonson, P. T. Springer, and R. Tommasini, "Fuel gain exceeding unity in an inertially confined fusion implosion," *Nature* **506**, pp. 343–348, 02 2014.
4. O. A. Hurricane, D. A. Callahan, D. T. Casey, E. L. Dewald, T. R. Dittrich, T. Döppner, M. A. Barrios Garcia, D. E. Hinkel, L. F. Berzak Hopkins, P. Kervin, J. L. Kline, S. L. Pape, T. Ma, A. G. MacPhee, J. L. Milovich, J. Moody, A. E. Pak, P. K. Patel, H.-S. Park, B. A. Remington, H. F. Robey, J. D. Salmonson, P. T. Springer, R. Tommasini, L. R. Benedetti, J. A. Caggiano, P. Celliers, C. Cerjan, R. Dylla-Spears, D. Edgell, M. J. Edwards, D. Fittinghoff, G. P. Grim, N. Guler, N. Izumi, J. A. Frenje, M. Gatu Johnson, S. Haan, R. Hatarik, H. Herrmann, S. Khan, J. Knauer, B. J. Kozioziemski, A. L. Kritcher, G. Kyrala, S. A. Maclaren, F. E. Merrill, P. Michel, J. Ralph, J. S. Ross, J. R. Rygg, M. B. Schneider, B. K. Spears, K. Widmann, and C. B. Yeamans, "The high-foot implosion campaign on the national ignition facilitya)," *Physics of Plasmas (1994-present)* **21**(5), pp. –, 2014.
5. J. A. Paisner, J. D. Boyes, S. A. Kumpan, W. H. Lowdermilk, and M. S. Sorem, "National ignition facility would boost united-states industrial competitiveness," *Laser Focus World* **30**, pp. 75–77, 1994.
6. A. C. Hayes, P. A. Bradley, G. P. Grim, G. Jungman, and J. B. Wilhelmy, "Reaction-in-flight neutrons as a signature for shell mixing in national ignition facility capsules," *Physics of Plasmas* **17**(1), p. 012705 (6 pp.), 2010.
7. Maynard, G. and Deutsch, C., "Born random phase approximation for ion stopping in an arbitrarily degenerate electron fluid," *J. Phys. France* **46**(7), pp. 1113–1122, 1985.
8. H. Azechi, M. D. Cable, and R. O. Stapf, "Review of secondary and tertiary reactions, and neutron scattering as diagnostic techniques for inertial confinement fusion targets," *Laser and Particle Beams* **9**, pp. 119–134, 3 1991.

9. M. B. Nelson and M. D. Cable, "Lansa: A large neutron scintillator array for neutron spectroscopy at nova," *Review of Scientific Instruments* **63**(10), pp. 4874–4876, 1992.
10. P. A. Bradley, G. P. Grim, A. C. Hayes, G. Jungman, R. S. Rundberg, J. B. Wilhelmy, G. M. Hale, and R. C. Korzekwa, "Neutron reactions in the hohlraum at the llnl national ignition facility," *Phys. Rev. C* **86**, p. 014617, Jul 2012.
11. V. Glebov, D. Meyerhofer, T. Sangster, C. Stoeckl, S. Roberts, C. Barrera, J. Celeste, C. Cerjan, L. Dauffy, D. Eder, R. Griffith, S. Haan, B. Hammel, S. Hatchett, N. Izumi, J. Kimbrough, J. Koch, O. Landen, R. Lerche, B. MacGowan, M. Moran, E. Ng, T. Phillips, P. Song, R. Tommasini, B. Young, S. Caldwell, G. Grim, S. Evans, J. Mack, T. Sedillo, M. Wilke, D. Wilson, C. Young, D. Casey, J. Frenje, C. Li, R. Petrasso, F. Seguin, J. Bourgade, L. Disdier, M. Houry, I. Lantuejoul, O. Landoas, G. Chandler, G. Cooper, R. Leeper, R. Olson, C. Ruiz, M. Sweeney, S. Padalino, C. Horsfield, and B. Davis, "Development of nuclear diagnostics for the national ignition facility (invited)," *Review of Scientific Instruments* **77**(10), pp. 10E715–1–7, 2006.
12. M. G. Johnson, J. A. Frenje, D. T. Casey, C. K. Li, F. H. Séguin, R. Petrasso, R. Ashabranner, R. M. Bionta, D. L. Bleuel, E. J. Bond, J. A. Caggiano, A. Carpenter, C. J. Cerjan, T. J. Clancy, T. Doeppner, M. J. Eckart, M. J. Edwards, S. Friedrich, S. H. Glenzer, S. W. Haan, E. P. Hartouni, R. Hatarik, S. P. Hatchett, O. S. Jones, G. Kyrala, S. L. Pape, R. A. Lerche, O. L. Landen, T. Ma, A. J. MacKinnon, M. A. McKernan, M. J. Moran, E. Moses, D. H. Munro, J. McNaney, H. S. Park, J. Ralph, B. Remington, J. R. Rygg, S. M. Sepke, V. Smalyuk, B. Spears, P. T. Springer, C. B. Yeamans, M. Farrell, D. Jasion, J. D. Kilkenny, A. Nikroo, R. Paguio, J. P. Knauer, V. Y. Glebov, T. C. Sangster, R. Betti, C. Stoeckl, J. Magoon, M. J. Shoup, III, G. P. Grim, J. Kline, G. L. Morgan, T. J. Murphy, R. J. Leeper, C. L. Ruiz, G. W. Cooper, and A. J. Nelson, "Neutron spectrometry—an essential tool for diagnosing implosions at the national ignition facility (invited)," *Review of Scientific Instruments* **83**(10), p. 10D308, 2012.
13. R. J. Leeper, G. A. Chandler, G. W. Cooper, M. S. Derzon, D. L. Fehl, D. E. Hebron, A. R. Moats, D. D. Noack, J. L. Porter, L. E. Ruggles, C. L. Ruiz, J. A. Torres, M. D. Cable, P. M. Bell, C. A. Clower, B. A. Hammel, D. H. Kalantar, V. P. Karpenko, R. L. Kauffman, J. D. Kilkenny, F. D. Lee, R. A. Lerche, B. J. MacGowan, M. J. Moran, M. B. Nelson, W. Olson, T. J. Orzechowski, T. W. Phillips, D. Ress, G. L. Tietbohl, J. E. Trebes, R. J. Bartlett, R. Berggren, S. E. Caldwell, R. E. Chrien, B. H. Failor, J. C. Fernandez, A. Hauer, G. Idzorek, R. G. Hockaday, T. J. Murphy, J. Oertel, R. Watt, M. Wilke, D. K. Bradley, J. Knauer, R. D. Petrasso, and C. K. Li, "Target diagnostic system for the national ignition facility (invited)," *Review of Scientific Instruments* **68**(1), pp. 868–879, 1997.
14. Y. Kim, J. M. Mack, H. W. Herrmann, C. S. Young, G. M. Hale, S. Caldwell, N. M. Hoffman, S. C. Evans, T. J. Sedillo, A. McEvoy, J. Langenbrunner, H. H. Hsu, M. A. Huff, S. Batha, C. J. Horsfield, M. S. Rubery, W. J. Garbett, W. Stoeffl, E. Grafil, L. Bernstein, J. A. Church, D. B. Sayre, M. J. Rosenberg, C. Waugh, H. G. Rinderknecht, M. Gatu Johnson, A. B. Zylstra, J. A. Frenje, D. T. Casey, R. D. Petrasso, E. K. Miller, V. Y. Glebov, C. Stoeckl, and T. C. Sangster, "Determination of the deuterium-tritium branching ratio based on inertial confinement fusion implosions," *Phys. Rev. C* **85**, p. 061601, Jun 2012.
15. S. R. Taylor and S. M. McClennan, *The Continental Crust: Its Composition and Evolution*, Blackwell Scientific Publications, 1985.